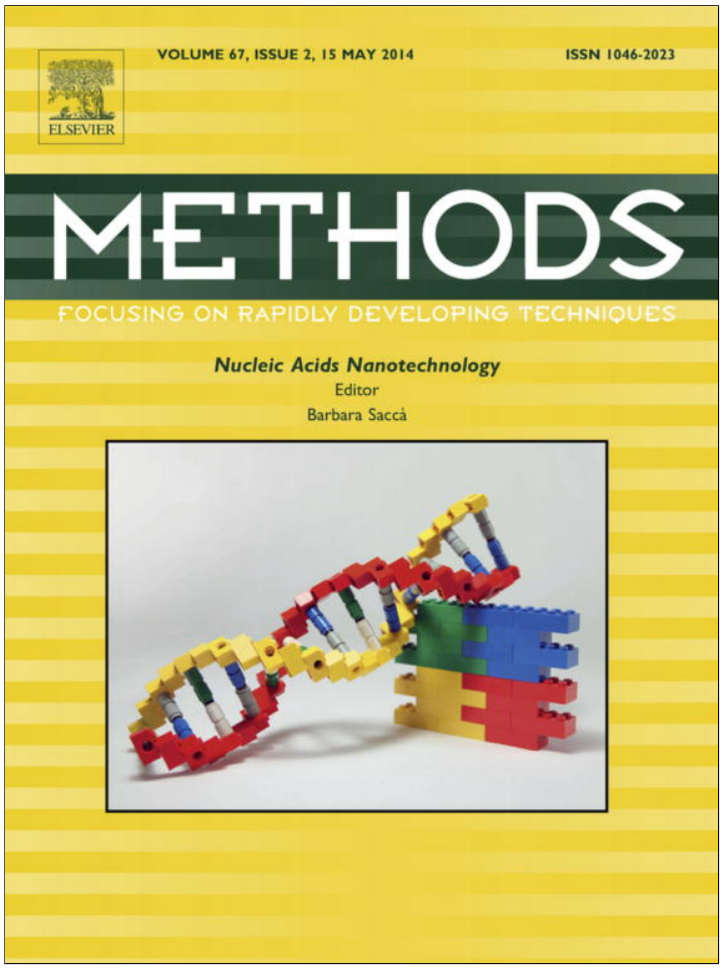

Methods 67 (2014) 177–184

Contents lists available at ScienceDirect

Methods

journal homepage: www.elsevier.com/locate/ymeth

Discovering anomalous hybridization kinetics on DNA nanostructures using single-molecule fluorescence microscopy

Alexander Johnson-Buck, Nils G. Walter *

Department of Chemistry, Single Molecule Analysis Group, 930 N. University Avenue, University of Michigan, Ann Arbor, MI 48109-1055, United States

ARTICLE INFO

Article history:
Available online 3 March 2014

Keywords:
Single-particle fluorescence resonance energy transfer
Points accumulation for imaging in nanoscale topography
Hybridization kinetics
DNA origami
DNA nanotechnology

ABSTRACT

DNA nanostructures are finding diverse applications as scaffolds for molecular organization. In general, components such as nucleic acids, proteins, and nanoparticles are attached to addressable DNA nanostructures via hybridization, and there is interest in exploiting hybridization for localized computation on DNA nanostructures. This report details two fluorescence microscopy methods, single-particle fluorescence resonance energy transfer (spFRET) and DNA-PAINT (points accumulation for imaging in nanoscale topography), that have been successfully used to detect anomalies of hybridization reactions on individual DNA nanostructures. We compare and contrast the two techniques, highlighting their respective strengths in studying equilibrium and non-equilibrium hybridization as well as assessing the variability of behaviors within individual nanostructures and across a population of nanostructures.

1. Introduction

In the past decade, structural DNA nanotechnology has emerged as a powerful tool for the organization of molecular components with nanometer precision. In particular, the DNA origami technique [1] has been used to build molecular automata [2–4], synthetic multi-enzyme complexes [5], and photonic devices [6–8] and has been proposed as a scaffold for molecular logic circuits [1,9] in the context of DNA computing [10,11]. All of these applications exploit the ability to attach nucleic acids, proteins, or nanoparticles to specific sites on the structural DNA scaffold, usually by hybridization of complementary DNA sequences. Successful execution of these approaches thus hinges on understanding what factors influence hybridization reactions at the surface of DNA nanostructures, especially when the yield and fidelity of intended processes depend on the kinetics of hybridization.

Hybridization to DNA nanostructures has been probed using a variety of techniques, including atomic force microscopy (AFM) [1,4,12], ensemble fluorescence or fluorescence resonance energy transfer (FRET) [13], and native gel electrophoresis. The total internal reflection fluorescence (TIRF) microscopy techniques single-particle FRET (spFRET) [14,15] and DNA-PAINT [16,17] provide high spatiotemporal resolution and low invasiveness that are particularly conducive to detailed studies of hybridization on single nanoscale complexes (Fig. 1). In our implementation of spFRET, a DNA target labeled with a FRET donor is allowed to saturate multiple acceptor-labeled probe sites on a single nanostructure, resulting in a large increase in acceptor fluorescence (Fig. 1A). This implementation of spFRET is well-suited to the non-equilibrium study of binding to many sites on single nanostructures, forgoing super-resolution spatial information in favor of simplicity, greater dynamic range, and less stringent sensitivity requirements than typical single-molecule techniques. In DNA-PAINT, by contrast, the reversible binding of single fluorescently labeled target oligonucleotides to individual probes on nanostructures is monitored over multiple binding cycles, yielding super-resolution spatial information about the kinetics of hybridization to various sites on each nanostructure (Fig. 1A). Unlike spFRET, DNA-PAINT depends on single-fluorophore sensitivity, but requires fluorescent labeling only of extrinsic target strands, thus rendering multicolor imaging more feasible.

Recently, we reported the use of spFRET [15] and DNA-PAINT [17] to characterize the kinetics of hybridization to ssDNA probes on DNA origami, demonstrating several differences from canonical solution behavior when the origami-bound probes are closely spaced. In this work, we present detailed protocols for these two techniques, as well as a comparison of their instrumentation and sample requirements and strengths in assessing different aspects of hybridization to DNA nanostructures (summarized in Fig. 1B).

Abbreviations: spFRET, single-particle FRET; PAINT, points accumulation for imaging in nanoscale topography; OSS, oxygen scavenger system.

* Corresponding author. Fax: +1 734 615 5524.
E-mail addresses: alebuck@umich.edu (A. Johnson-Buck), nwalter@umich.edu (N.G. Walter).

http://dx.doi.org/10.1016/j.ymeth.2014.02.032
1046-2023/

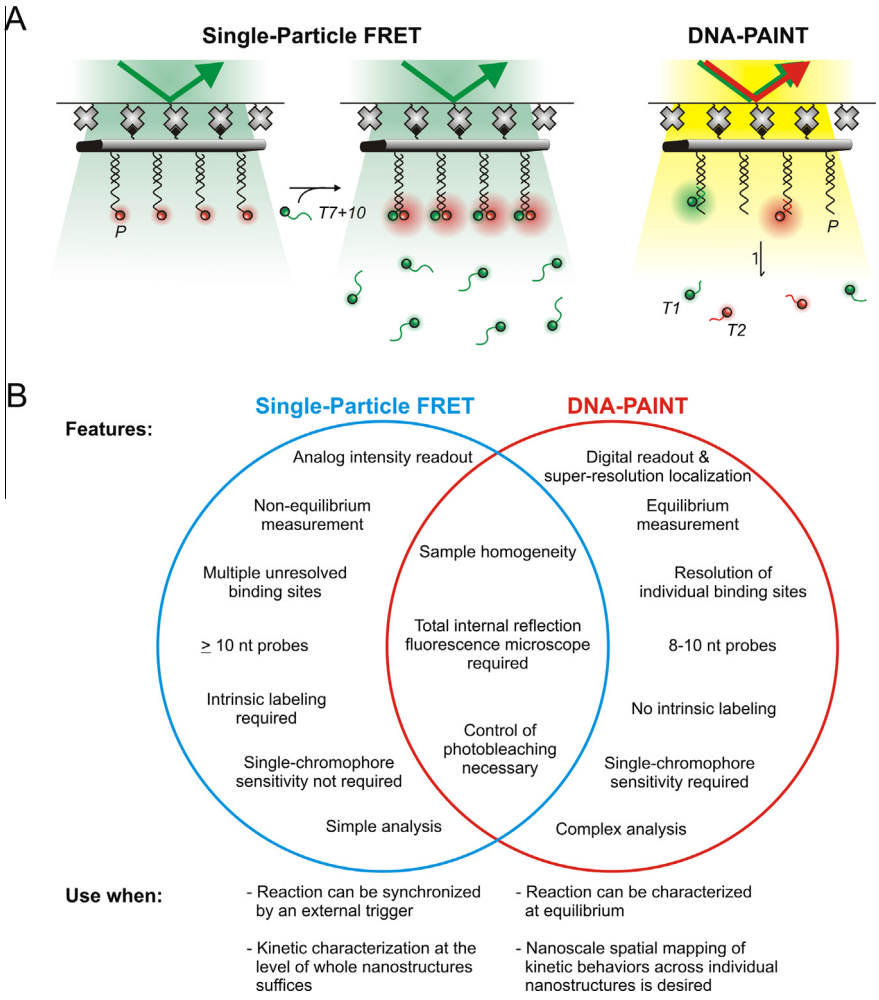

Fig. 1. Overview of techniques. (A) Schematic illustration of studying hybridization to single DNA origami by spFRET and DNA-PAINT. Nanostructures are labeled with biotin (black diamonds) to permit immobilization on a glass surface coated with streptavidin or NeutrAvidin (gray crosses). (B) Comparison of the features and capabilities of spFRET and DNA-PAINT.

2. Materials and methods

2.1. Microscope

Both spFRET and DNA-PAINT require a microscope capable of TIRF or HILO [18] illumination to reject background signal from unbound fluorescent probes. A schematic of the microscope used in this study is shown in Fig. 2A. Excitation is provided by two diode lasers: a CrystaLaser CL532-050-L (532 nm, 50 mW) for Cy3 excitation, and an Olympus LAS/640/100-D (640 nm, 100 mW) for Cy5 excitation. In the case of spFRET measurements, only the green (532 nm) laser is used, and is attenuated using a neutral-density filter (optical density of 1.0) to minimize photobleaching, which would interfere with kinetics measurements. Using a series of mirrors and a focusing lens, the excitation beams are directed to a prism lying on top of the microscope slide containing the sample, where they undergo total internal reflection at the slide-solution interface (Fig. 1A), exciting fluorophores within ~100 nm of the slide surface. The fluorescence emission is passed through a 60× objective and an optional 1.6× magnifier (used in DNA-PAINT for increased spatial resolution). The image is cropped by passing through a narrow slit, then split into two frequency bands, or channels, using a dichroic mirror with a cutoff wavelength of 610 nm (Chroma). Using a series of mirrors and lenses, each of the two image channels is focused onto one half of an intensified CCD camera chip (iPentamax HQ Gen III, Roper Scientific, Inc.). A Newport ST-UT2 vibration isolation table is used in all experiments to reduce instrument interference.

2.2. Fluorescent target design

DNA-PAINT and spFRET impose somewhat different constraints on the design of single-stranded DNA (ssDNA) probe–target interactions. For non-equilibrium spFRET measurements, targets must be long enough (typically ⩾ 10 nt) to ensure a small dissociation constant (preferably < 10 nM), which allows the binding sites to be highly populated without increasing target concentrations beyond ~100 nM, at which point background signal from unbound target may become problematic. For the spFRET assays described here, we use an 8–17 deoxyribozyme target *T7+10-Cy3* (5′-/5Cy3/TCT CTT CTC CGA GCC GGT CGA AAT AGT GAA AA) and a probe sequence *P* (5′-GAT GAA TGG TGG GTG AGA GGT TTT TCA CTA TrAG GAA GAG), which is a substrate for the 8–17 deoxyribozyme [19]. Importantly, since our conditions contain no divalent metal cations, no substrate cleavage occurs on the timescale of our experiments. For spFRET, *P* is modified with Alexa Fluor 647 (AF647) at its 3′-end to act as a FRET acceptor upon binding. For dissociation reactions, we use an unlabeled *P* strand to sequester target as it dissociates from the nanostructures. We also investigate the dissociation of a second target, *T11O*-Cy3 (5′-/5Cy3/TCT CTT CCT ATA

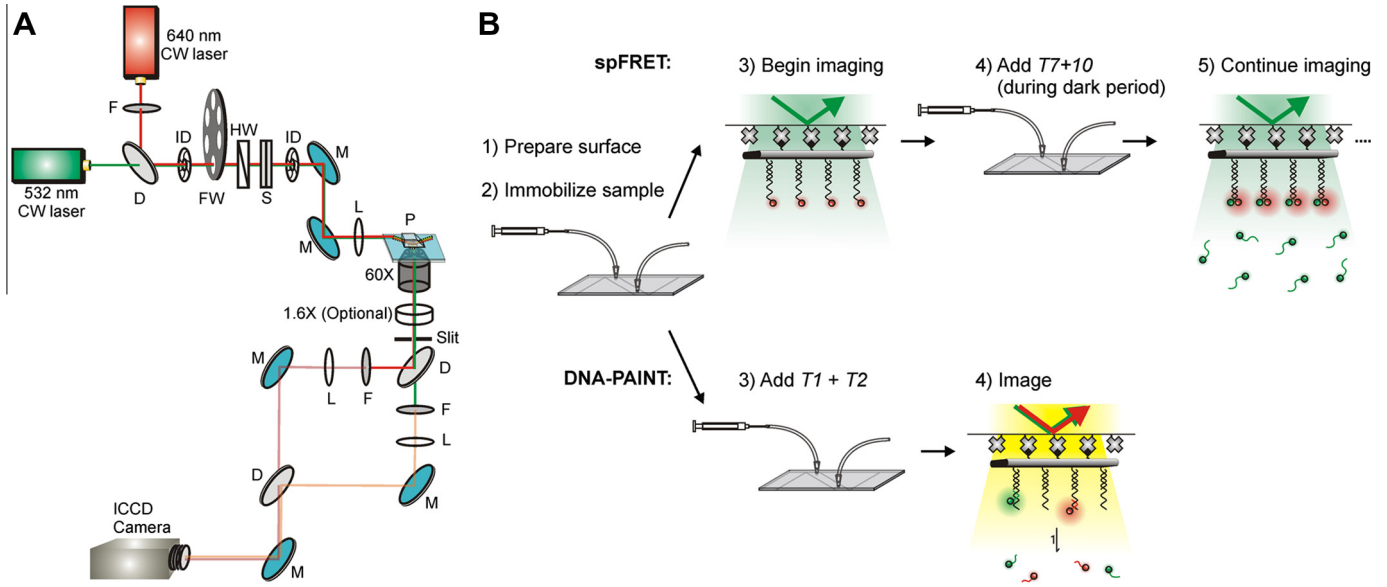

Fig. 2. (A) Total internal reflection fluorescence (TIRF) microscope used in this study. Key: F = filter, D = dichroic mirror, ID = iris diaphragm, FW = filter wheel, HW = half-wave plate, S = shutter, M = mirror, L = lens, P = prism. (B) Schematic of sample preparation and data acquisition in spFRET and DNA-PAINT experiments.

CGC TGA AAG GTG ACG GCA AA) from *P*-AF647, with which it forms an 11-base-pair duplex.

For DNA-PAINT, reversible binding is required to allow for many cycles of binding and dissociation on the same nanostructure. In practice, this means that the target must typically form between 8 and 10 base pairs with the probe on the DNA nanostructure; however, this will depend on both ionic strength and the sequence of the complementary region, and a few different target lengths should be tested under the imaging conditions for optimal performance. The lifetime of the bound state should be longer than the exposure time (in this case, 1 s) but not so long as to encumber the observation of many temporally separated binding events during the experimental time frame. In our case, the 9-nucleotide targets *T1*-Cy5 (5′-Cy5-CTC TTC CTA) and *T2*-Cy3 (5′-Cy3-ATA GTG AAA) are used to bind two different segments of the same probe *P*.

2.3. Preparation of nanostructures

For this study, DNA origami nanostructures are prepared with between 12 and 187 copies of *P* as previously described [15,17]. Briefly, a modification of the one-pot thermal annealing protocol by Rothemund [1] is first used to assemble the DNA origami scaffold; several staples are modified to display a capture sequence (5′-CCT CTC ACC CAC CAT TCA TC) on one face of the origami tile. Five staples are also modified to display biotins on the opposite face of the tile for purposes of surface immobilization. Prior to each experiment, a $\geqslant$2-fold excess of *P* or *P*-A647 is allowed to hybridize to the capture sequence at room temperature for 5–10 min. Optionally, excess oligonucleotides may be removed by ultrafiltration through an Amicon UltraCel 100 kDa cutoff filter (Millipore). In the experiments described here, excess oligonucleotides are simply flushed away by buffer injection after immobilizing the origami on the microscope slide surface (Sections 2.6 and 2.8).

2.4. Slide preparation

Fused silica microscope slides (Finkenbeiner, 1 in. × 3 in. × 1 mm) are coated with streptavidin or NeutrAvidin to permit the immobilization of biotin-labeled nanostructures for TIRF observation. For spFRET experiments, as described previously [14,20], a fluidic channel is created by sandwiching two pieces of double-sided tape (Scotch) between the microscope slide and a coverslip (VWR, 48404-466), creating a ~3 mm-wide channel between two 1-mm holes that have been drilled into the slide. Immediately before imaging, to allow for easy injection of samples and buffer exchange, injection and waste ports are added by attaching plastic tubing (Tygon, 0.020′ ID, 63018-044) to the holes in the slide using cut segments of plastic pipet tips (Eppendorf) and epoxy adhesive (Hardman Adhesives, 04001). The bare glass surface is then coated with streptavidin using a protocol [14] in which 1 mg/mL biotinylated BSA (Thermo Fisher, 29130) is adsorbed onto the slide surface for 10 min, followed by washing with T50 buffer (10 mM Tris–HCl, 50 mM NaCl, pH 8.0), incubation with 0.2 mg/mL streptavidin for 10 min, and flushing with imaging buffer.

For DNA-PAINT experiments, it is important to create a denser coating to enable each origami tile to attach via multiple biotins so that it will lie flat on the surface and not rotate [21]. We therefore employ a protocol [2,20] in which the glass surface of the slide is covalently modified with (3-aminopropyl)triethoxysilane followed by the addition of the bisfunctional cross-linking agent *para*-diisothiocyanatobenzene, to which NeutrAvidin (Invitrogen, A2666) is in turn directly conjugated. NeutrAvidin was used in DNA-PAINT experiments due to its more neutral isoelectric point compared to that of streptavidin, which we find to reduce nonspecific binding of charged species such as DNA oligonucleotides to the slide surface (unpublished data). After construction of a flow channel as described above, the slides are stored under vacuum at 4 °C for up to 4 weeks before use. As with spFRET experiments, Tygon tubing is attached to the slide facilitate buffer exchange prior to imaging.

2.5. Buffers and oxygen scavenger

All imaging is performed in 1 × HBS (50 mM HEPES-KOH, pH 7.2–7.4, 150 mM NaCl). While DNA origami assembly is optimal in the presence of magnesium or high concentrations of monovalent cations, we find the origami used in this study to be stable for several hours at room temperature in 1 × HBS as determined by atomic force microscopy, provided that it is first annealed at higher ionic strength (300–500 mM NaCl or 10–12 mM $MgCl_2$) [17]. In addition, the photobleaching of fluorophores is retarded by supplementing *all imaging buffers* with an oxygen scavenger

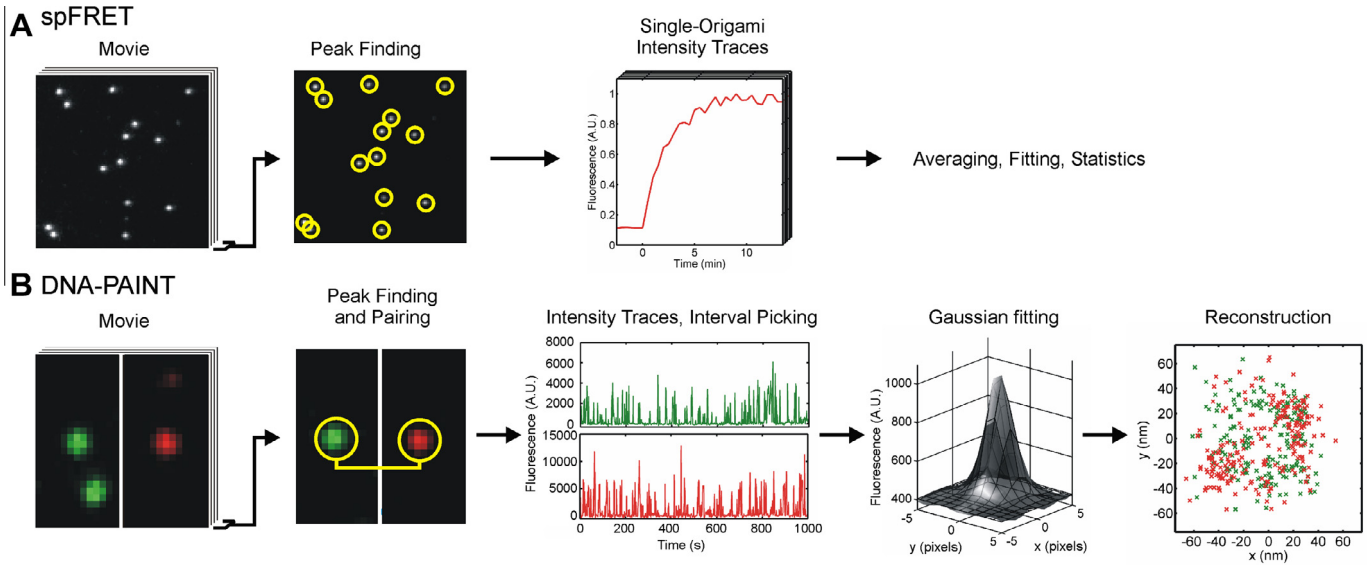

Fig. 3. Workflow for analysis of spFRET and DNA-PAINT data. (A) spFRET: the raw movie is averaged to localize each origami tile with high precision. Intensity traces are generated from each diffraction-limited spot, correcting for microscope stage drift, and subjected to kinetic analysis as described in Section 2.7.3. (B) DNA-PAINT: a fluctuation map is generated from the raw movie to identify the regions of repeated binding of targets. Corresponding regions of repeated binding in the two frequency channels are registered and paired as described in Section 2.8.3. Intensity traces are generated, and thresholding is used to identify the time intervals in which a target is bound. Such intervals are subjected to 2-D Gaussian fitting, and the resulting coordinates are plotted to yield a reconstruction of the underlying field of binding sites.

system (OSS) consisting of 2.5 mM 3,4-dihydroxybenzoic acid (Sigma, P5630), 1 mM Trolox (Acros, 218940050), and 25 nM protocatechuate dioxygenase (Sigma–Aldrich, P8279). The extent of photobleaching as a function of cumulative exposure to excitation light accounts for <10% of the decrease in fluorescence seen in the slowest reaction presented in this study, as determined by continuous illumination of DNA origami (~5 nm spacing) bound to *T7+10* in the absence of the chase strand (Fig. 4C).

2.6. Measurement of hybridization kinetics using spFRET

All imaging is performed at an environmentally controlled temperature of 20 °C. Injections are performed with plastic syringes (Becton, Dickinson & Co., 309659 & 305122). Sample preparation is performed as follows:

- Introduce 200 μL of a solution containing 20–100 pM origami in 1 × HBS into the fluidic channel of a biotinylated BSA/streptavidin-coated microscope slide and incubate for 10 min.
- Flush away excess sample by two 200-μL washes with 1 × HBS.
- Add 200 μL of a solution of 200 nM *P*-AF647 (acceptor-labeled probe) to the slide channel and incubate for 15 min before flushing the excess away by two 200-μL washes with 1 × HBS.
- Wait 3–5 min for the OSS to equilibrate.
- Prior to beginning FRET measurements, briefly focus on and locate origami using the fluorescence of AF647 resulting from cross-excitation by the 532-nm laser. Discontinue illumination and wait ~1 min for the microscope focus to relax; if necessary, quickly re-focus and repeat until the focus is stable.

2.6.1. Association kinetics

Association kinetics measurements are performed as follows:

- To reduce photobleaching, a shuttered illumination scheme is used: the sample is illuminated at 532 nm for 0.5-s intervals separated by 29.5-s dark periods.
- After an initial waiting period to establish a signal baseline (typically ~2 min is sufficient), add 200 μL of a solution of 25, 50, 75, or 100 nM *T7+10-Cy3* in imaging buffer to the slide during the beginning of a dark period (injection time ~ 5 s).
- Monitor the increase in AF647 fluorescence; continue measurement until the intensity stabilizes, signifying that equilibrium has been reached. In our system, FRET from Cy3 to AF647 results in an approximately 5-fold net increase in AF647 fluorescence upon binding of the target to the probe.

2.6.2. Dissociation kinetics

Dissociation kinetics measurements are performed as follows:

- For dissociation kinetics experiments, the length of dark periods in between acquisitions is increased to 119.5 s due to the longer time required for the dissociation of *T7+10-Cy3*. The dark interval should be short enough to capture the dissociation kinetics at sufficient resolution for accurate fitting, but long enough to prevent significant photobleaching during the observation window. The same exposure time of 0.5 s is used.
- Begin image acquisition. During a dark period, inject 200 μL of a solution of 500 nM unlabeled probe as a chase to prevent re-binding of dissociated *T7+10-Cy3*.

2.7. Analysis of spFRET data

2.7.1. Peak finding and generation of intensity traces

Intensity analysis of origami is performed using custom routines written in MATLAB (available on request) that perform the following:

- Combine all movie frames from the A647 channel to create an averaged image.
- In the averaged image, find local intensity maxima. To minimize the likelihood that two origami will be counted as one, each fluorescent spot ("point-spread function," or PSF) may be subjected to 2-D Gaussian fitting and rejected if it exceeds certain criteria of width or symmetry.

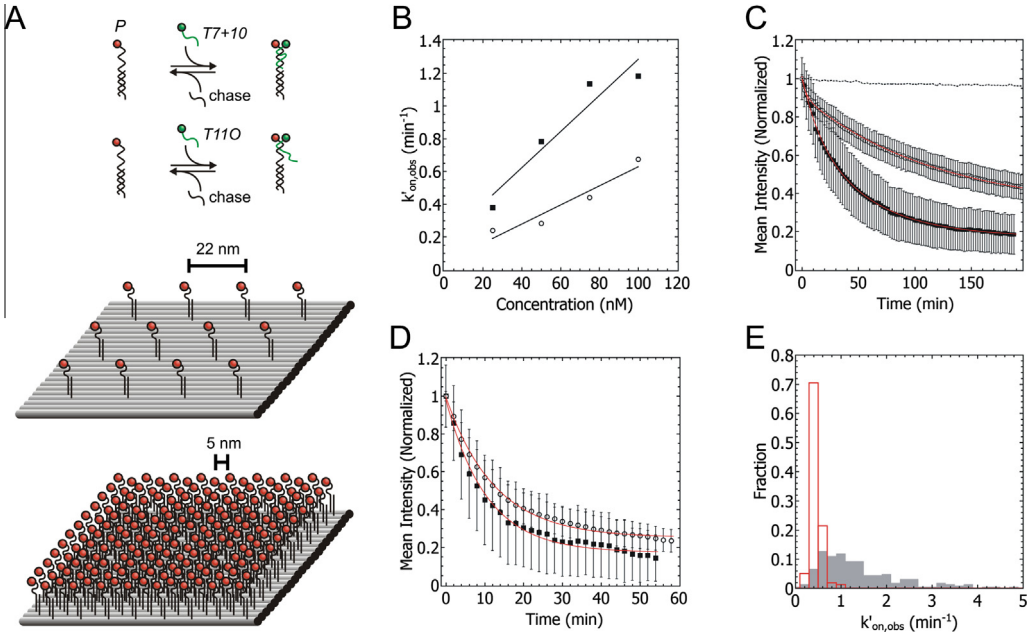

Fig. 4. spFRET measurements of hybridization kinetics. (A) Top: scheme of target binding and dissociation experiments using two different target sequences with different modes of binding to the probe *P*. Bottom: origami tiles used in spFRET measurements, with ~22 or ~5 nm between adjacent probes. (B) Linear fits of pseudo-first-order rate constants of *T7+10* binding to origami with a spacing of ~5 nm (circles) or ~22 nm (squares) between nearest-neighbor probes as a function of target concentration. The pseudo-first-order rate constants are derived from single-exponential fits to intensity versus time traces derived from averages of multiple origami tiles (see Table 1). (C) Kinetics of *T7+10* dissociation from origami with a spacing of ~5 nm (circles) or ~22 nm (squares) between nearest-neighbor probes. The red lines represent double-exponential fits of the mean intensity traces. The dashed line represents the extent of photobleaching of the AF647 label with *P* bound to *T7+10* on DNA origami under continuous illumination with the same intensity and overall duration as the dissociation measurements. Error bars in (C) and (D) represent one standard deviation across a population of >100 individual origami tiles (see Table 1). (D) Kinetics of *T11O* dissociation from origami with a spacing of ~5 nm (circles) or ~22 nm (squares) between nearest-neighbor probes. The red lines represent single-exponential fits of the intensity traces. (E) Histograms of apparent pseudo-first-order association rate constants of 75 nM *T7+10* binding to individual origami with ~5 nm (red) or ~22 nm (gray) between adjacent probes.

- To generate intensity versus time traces, calculate the A647 fluorescence emission intensity of each origami in each movie frame by summing the counts in a 5-by-5 pixel region centered on the pixel of locally maximal intensity, and then subtracting the median (background intensity) value of the 24 pixels immediately surrounding this region. If the microscope stage drifts by more than one pixel during the measurement, the 5-by-5 pixel region must be redefined in each frame to account for this drift prior to calculating the intensity (see Section 2.7.2).

2.7.2. Correction of microscope stage drift

During the course of a kinetic measurement (30–300 min), our microscope stage drifts by typically 1–3 pixels in the *x*- and/or *y*-direction. To correct for this drift, the following procedure is followed in MATLAB (software available upon request):

- Each movie of *N* frames is divided into 5–10 bins, each containing *N*/10 to *N*/5 frames. All the frames within each bin are averaged to create a consensus image for that time interval.
- The consensus image from the first bin is cross-correlated with that of each subsequent bin in the movie using the MATLAB function dftregistration [22], yielding an estimate of the net displacement of the field of view over time.
- Linear interpolation is used to estimate the microscope stage drift in each movie frame. This drift term is added to the original coordinates of each origami tile prior to calculation of its intensity.

2.7.3. Kinetic analysis

- To correct for inhomogeneity of illumination across the field of view, the fluorescence intensity of each origami tile is normalized to its maximal value in a given experiment.
- The mean intensity per origami tile is plotted as a function of time and fit with exponential decay models. In the case of association reactions, the data are fit by the single-exponential decay function $y = C\left(1 - e^{k'_{obs}t}\right)$ to obtain pseudo-first-order rate constants at each concentration. These pseudo-first-order rate constants are then plotted as a function of concentration and fit with a straight line (Fig. 4B) to estimate the true second-order rate constant of binding.
- The apparent rate constants for reactions on single origami tiles are estimated by fitting a single exponential decay function to individual (non-averaged) intensity versus time traces.

2.8. Measuring spatial heterogeneity of binding by two-color DNA-PAINT

- Introduce 200 μL of 100 pM origami sample into the channel of a NeutrAvidin-coated slide, and allow to bind for 10 min.
- Flush away excess sample by two washes with 1 × HBS.
- Mount the slide on the TIRF microscope, and add 200 μL of a solution containing 1 × HBS, OSS, and 10–20 nM of *T1*-Cy5 and *T2*-Cy3 to the slide channel.
- After waiting 2–5 min to allow equilibration of the OSS, visualize the binding of the PAINT targets under excitation at 532 nm and 640 nm with a camera capture rate of 1 Hz.

Continue imaging until enough binding events are observed to ensure a high probability of sampling each binding site on the nanostructure (in this study, 2000–4000 s, or 100–200 binding events per target [17]).

2.9. Analysis of DNA-PAINT data

2.9.1. Particle finding

Individual origami tiles are located in the field of view by the repeated appearance of Cy3 and/or Cy5 signal in the same location:

- A fluctuation map is generated by subtracting each movie frame from the preceding frame, taking the absolute value of the intensity differences, and averaging across all movie frames to obtain the average frame-to-frame fluctuation in intensity at each pixel. This permits us to distinguish origami, as sites of repeated PAINT probe binding, from occasional bright fluorescent contaminants.
- The origami tiles, which appear as bright diffraction-limited spots in this fluctuation map, are localized by Gaussian fitting to obtain coordinates of each origami in a field of view (Fig. 3B).
- For each origami, traces of intensity as a function of time (Fig. 3B) are generated as described in Section 2.7.1. During the generation of intensity traces, the 5-by-5 pixel region is re-defined if the microscope stage drifts by more than one pixel in the x or y direction (see Section 2.7.2).

2.9.2. Localization analysis

- During movie frames in which a DNA origami's fluorescence intensity exceeds a threshold number of counts above background (500–2000 photons/s, depending on the experiment and excitation intensity), the intensity profile is fit with a 2-dimensional Gaussian function of the form:

$$I = Ce^{-\frac{(x-\mu_x)^2}{2\sigma_x^2}-\frac{(y-\mu_y)^2}{2\sigma_y^2}} + b \quad (1)$$

to extract the centroid (μ_x,μ_y), as well as parameters for localization error estimation, including PSF widths σ_x and σ_y and a more precise photon count ($2\pi C\sigma_x\sigma_y$). A 7 × 7-pixel fitting box centered on the origami is used for fitting.

- Gaussian fits are filtered for quality and rejected if any of the following criteria are met:
  1. Either σ_x or σ_y exceeds a cutoff of 2 pixels (266 nm).
  2. The residual between the fit and the actual intensity profile within the fitting box exceeds 25% of the total integrated counts of the Gaussian curve within the fitting box.
- This helps to reduce the influence of aberrant fits resulting from nonspecific binding of probes to the slide surface in the vicinity of the origami.
- Fitting error is estimated as described [23], using the parameters derived from each fit as well as the standard deviation of the background signal and the effective pixel size of 133 nm, determined using an objective micrometer.
- To avoid duplicate counting of a single binding event lasting multiple frames, multiple fits from the same binding event are combined by taking the median of all centroid measurements ($\mu_{x,i}$,$\mu_{y,i}$) for that event.

2.9.3. Reconstruction

To generate PAINT reconstructions:

- All position measurements (μ_x,μ_y) for an origami are enumerated.
- The microscope stage drift in the corresponding movie frame is subtracted from each position measurement.
- A reconstruction is generated as a sum of Gaussian functions on a grid of 3- to 4-nm square pixels, with the centroid of each Gaussian representing a drift-corrected position measurement. The width parameters σ_x and σ_y for the reconstruction Gaussians are defined as the median error for all position measurements for a given origami.

2.9.4. Registration

For two-color PAINT reconstructions, the binding distributions of *T1-Cy5* and *T2-Cy3* binding must be registered into the same coordinate space due to inevitable chromatic aberrations resulting from the separate light path followed by each image channel. These aberrations are corrected for in the following manner:

- First, a coarse third-order polynomial mapping is found between the two channels using Gaussian fitting of fiduciary markers with fluorescence visible in both channels (FluoSpheres 580/605, Invitrogen, F-8810). Our registration error [24], calculated as the average distance between the calculated and actual positions of the Cy5 centroid based on the polynomial mapping from Cy3 coordinates, is 10–20 nm. An initial two-color overlay of the PAINT reconstructions is generated using this coarse mapping.
- To further fine-tune the registration, the PAINT reconstructions from Cy3 and Cy5 are registered directly by cross-correlation [22]. To reduce the influence of uneven binding (heterogeneous binding or sampling noise) on registration, the reconstruction in each channel is saturated at 10% of its maximal intensity value for purposes of registration.

3. Results and discussion

3.1. Density-dependent dissociation and binding by spFRET

In an initial application of spFRET to investigate the influence of probe crowding on hybridization kinetics [15], we compared the hybridization kinetics of target *T7+10* to probe *P* on a rectangular DNA origami tile with two different spacings between nearest-neighbor probes: ~5 nm and 22 nm (Fig. 4A). We found that binding to origami with a 5-nm inter-probe spacing is approximately 1.9-fold slower than to origami with a 22-nm spacing (Fig. 4B and Table 1), suggesting that two-dimensional crowding of probes hinders binding through steric hindrance or probe–probe interactions that compete with binding of an external target. Similarly, the majority phase of dissociation of *T7+10* is 2.4-fold slower on the origami with a 5-nm spacing than on that with a 22-nm spacing (Fig. 4C and Table 1). Since *T7+10* binds to *P via* a multivalent interaction consisting of two helical arms, we hypothesize that this slowing of dissociation at high probe densities is the result of walking between adjacent probes. Indeed, the multivalent binding of related deoxyribozymes has been exploited to design molecular walkers that traverse a track [25] or carry out a multi-step synthesis [26]. In our system, the length of the double-helical segment anchoring each probe to the DNA origami is 20 nucleotides, or about 6.6 nm, which makes interactions between probes likely at a 5-nm spacing but unlikely at 22 nm.

To test the hypothesis that inter-probe walking slows dissociation, we measured the dissociation kinetics of a target, *T11O*, that binds to *P via* only a single, 11-nucleotide helical segment, but has the same length and base composition as *T7+10*. In contrast to *T7+10*, *T11O* dissociation is nearly unaffected by the spacing between adjacent probes (Fig. 4D), consistent with the hypothesis that *T7+10* dissociation is slowed by walking between probes on the origami surface. Furthermore, we have shown that when the

Table 1
Statistics and fit parameters for the binding and dissociation reactions studied by spFRET. Values shown are: N, number of origami; k_1 and k_2, apparent dissociation rate constants from single- or double-exponential fitting; A_1 and A_2, amplitudes of phases from exponential fitting; y_0, offset from exponential fitting; $k'_{on,obs}$, apparent pseudo-first-order rate constant from single-exponential fitting of association curves; $k_{on,obs}$, apparent second-order rate constant of association derived from linear fits as shown in Fig. 4B (error shown was derived from linear regression fit).

Probe	Probe spacing (nm)	N	k_1 (min^{-1})	A_1	k_2 (min^{-1})	A_2	y_0
Dissociation kinetics							
T7+10	5	156	0.0079	0.60	0.13	0.090	0.30
	22	496	0.019	0.61	0.072	0.24	0.17
T11O	5	436	0.080	0.75	–	–	0.25
	22	240	0.095	0.81	–	–	0.17

T7+10 Association kinetics

Probe spacing (nm)	[T7+10] (nM)	N	$k'_{on,obs}$ (min^{-1})	$k_{on,obs}$ (M^{-1} s^{-1})
5	25	23	0.24	0.97 ± 0.20
	50	36	0.28	
	75	159	0.44	
	100	45	0.67	
22	25	566	0.38	1.84 ± 0.39
	50	529	0.78	
	75	461	1.14	
	100	171	1.18	

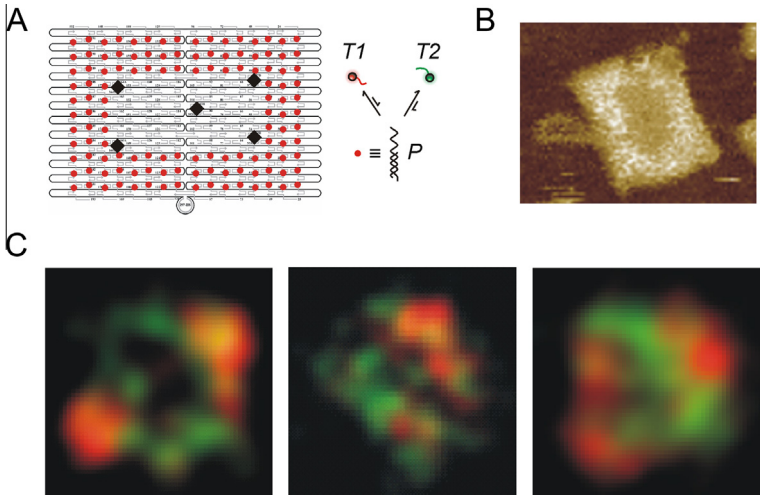

Fig. 5. Heterogeneity of *T1* binding to a rectangular pattern of probes. (A) Design of DNA origami bearing a rectangular arrangement of *P* strands (red dots) and five biotins for surface immobilization (black diamonds, opposite face of tile). (B) An AFM image of the formed structure. (C) Two-color DNA-PAINT reconstructions of rectangular patterns of *P* strands on DNA origami, illustrating the heterogeneous binding of *T1* (red) relative to *T2* (green). PAINT reconstructions are 125 nm × 125 nm.

majority of *P* is replaced by a randomized control sequence of the same length and base composition, reducing the likelihood that *T7+10* will find a second binding partner nearby, the dissociation of *T7+10* from a field of probes spaced by 5 nm increases ~3-fold [15]. Taken together, these results strongly suggest that walking of a target between closely spaced probes can have a significant impact on the overall rate of dissociation from DNA nanostructures.

3.2. Low variability of rate constants between origami tiles

In addition to characterizing the average kinetic behavior, we also examined the variability of rate constants among individual origami by fitting of single-origami intensity versus time traces [15]. We found that the rate constants of binding and dissociation vary by only 10–20% between origami tiles with a ~5 nm spacing between probes (Fig. 4E), most of which can be explained by stochasticity resulting from a small number of binding events and instrument noise [15]. Thus, despite local variability of kinetics on a single origami tile (see Section 3.3), the kinetics of hybridization as averaged over all probes on a given tile are highly reproducible within a population of tiles. Despite the possibility of assembly defects [1] and conformational flexibility [27], the kinetic behavior can be quite robust and, with ~200 probe–target reactions on a tile, nearly deterministic. This property may prove useful in DNA computing [10] by allowing for quasi-deterministic operations to be performed in a small localized space rather than by freely diffusing components in bulk solution. Not surprisingly, as the number of probes on a given tile is reduced by a factor of four (~22 nm spacing), the apparent rate constant of binding becomes more variable due to the small number of events ($\leqslant$12) per tile (Fig. 4E).

3.3. DNA-PAINT reveals sequence-specific spatial heterogeneity of binding on single origami tiles

By reconstructing the spatial binding patterns of *T1* and *T2* binding to a rectangular pattern of probes over 100–200 binding cycles per probe, we examined the homogeneity of binding kinetics over a single origami tile [17]. Since *T1* and *T2* bind to different segments of the same probe (*P*), we expected to observe the same pattern and relative frequency of binding (fraction of binding events within a given region) for both probes. However, as shown in Fig. 5, we in fact observe highly heterogeneous kinetics of *T1* binding over the tile surface. *T2* binds more homogeneously across the probe array. While the precise pattern of *T1* binding varies

somewhat from tile to tile, we often observe enriched binding to opposite corners of the tile (Fig. 5C). CanDo [27] modeling and further kinetics controls [17] suggest that this sequence-specific heterogeneity may be due to a combination of intrinsic curvature of the origami tile and weak probe–probe interactions that compete for *T1* binding. For instance, the region of *P* that is complementary to *T1* (see Section 2.2) contains a pair of consecutive guanine residues that, at the estimated 2–8 mM local concentration of probes, may form four-strand G-quadruplex structures that inhibit the binding of *T1* in corners of the tile that place nearest-neighbor *P* strands in close proximity.

4. Conclusions

Using spFRET and DNA-PAINT, we have shown that hybridization kinetics at the surface of DNA origami can deviate significantly from expected behavior, particularly in dense fields of probes [15,17]. Since many implementations of dynamic DNA nanotechnology [2,4,25] as well as possible future spatially organized molecular logic circuits [9] utilize closely spaced ssDNA components, it is important to understand to what extent the kinetic behavior of such components is affected by immobilization at the surface of a DNA nanostructure, and what parameters (scaffold topology, probe sequences, etc.) may require further optimization to avoid unintended interactions. From the standpoint of characterization, our results indicate that interactions between densely spaced probes on nanostructures may interfere with the fidelity of some kinetic assays. Future investigations may discover ways of mitigating or avoiding these issues, for example by omitting certain nucleobases from the probe sequences to minimize local interactions; or, the problem may simply be avoided by using probe densities and geometries that prevent interactions between adjacent surface-bound probes.

Single-particle FRET and DNA-PAINT provide means of acquiring detailed spatial, temporal, and population-level information about binding and dissociation kinetics on individual DNA nanostructures that should prove useful throughout all areas of DNA nanotechnology and molecular computing. The simplicity and high signal-to-noise of the spFRET technique render it an attractive option when reactions can be easily synchronized *via* an external trigger, and when the relevant kinetic behavior occurs at the level of the entire nanostructure or a population of nanostructures. When it is necessary to study equilibrium kinetic behaviors and their spatial distribution across an individual nanostructure, the somewhat more technically challenging DNA-PAINT technique is preferable. While it is theoretically possible to determine the exact number of DNA strands hybridized to a nanostructure by spFRET, for instance by counting the number of discrete intensity levels as individual targets sequentially bind, the dynamic range of the CCD detectors typically used in single-molecule microscopy is not sufficient to count large numbers of fluorescent molecules (>10) with single-molecule sensitivity, and photophysical processes such as blinking and photobleaching may interfere with the analysis. Alternatively, DNA-PAINT can be used to sequentially count individual molecules on a DNA scaffold [16,28], but in practice it is challenging to resolve probe sites separated by <20–30 nm due to imperfect correction of instrument drift. However, these limitations of both techniques are likely to diminish through the development of more photostable yet minimally invasive fluorophores, single-molecule-sensitive detectors with higher dynamic range, and improved hardware- and software-based methods for correcting instrument drift. We expect that the application of techniques such as spFRET and DNA-PAINT to the study of DNA nanostructures will facilitate the rational control of not only structural properties but also dynamic behaviors in DNA nanotechnology and beyond.

Acknowledgements

This work was funded in part by National Science Foundation (NSF) Collaborative Research award EMT/MISC CCF-0829579 and the Department of Defense MURI award W911NF-12-1-0420. A.J.B. acknowledges support from a Rackham Predoctoral Fellowship. The authors acknowledge Jeanette Nangreave, Shuoxing Jiang, Yang Yang, and Hao Yan for the design, preparation, and AFM characterization of DNA origami samples.

References

[1] P.W.K. Rothemund, Nature 440 (2006) 297–302.
[2] K. Lund, A.J. Manzo, N. Dabby, N. Michelotti, A. Johnson-Buck, J. Nangreave, et al., Nature 465 (2010) 206–210.
[3] H. Gu, J. Chao, S.-J. Xiao, N.C. Seeman, Nature 465 (2010) 202–205.
[4] S.F.J. Wickham, J. Bath, Y. Katsuda, M. Endo, K. Hidaka, H. Sugiyama, et al., Nat. Nanotechnol. 7 (2012) 169–173.
[5] J. Fu, M. Liu, Y. Liu, N.W. Woodbury, H. Yan, J. Am. Chem. Soc. 134 (2012) 5516–5519.
[6] A. Kuzyk, R. Schreiber, Z. Fan, G. Pardatscher, E.-M. Roller, A. Högele, et al., Nature 483 (2012) 311–314.
[7] G.P. Acuna, F.M. Möller, P. Holzmeister, S. Beater, B. Lalkens, P. Tinnefeld, Science 338 (2012) 506–510.
[8] X. Shen, A. Asenjo-Garcia, Q. Liu, Q. Jiang, F.J. García de Abajo, N. Liu, et al., Nano Lett. 13 (2013) 2128–2133.
[9] L. Qian, E. Winfree, Science 332 (2011) 1196–1201.
[10] L.M. Adleman, Science 266 (1994) 1021–1024.
[11] M. Stojanovic, D. Stefanovic, Nat. Biotechnol. 21 (2003) 1069–1074.
[12] Y. Ke, S. Lindsay, Y. Chang, Y. Liu, H. Yan, Science 319 (2008) 180–183.
[13] A.V. Pinheiro, J. Nangreave, S. Jiang, H. Yan, Y. Liu, ACS Nano 6 (2012) 5521–5530.
[14] R. Roy, S. Hohng, T. Ha, Nat. Methods 5 (2008) 507–516.
[15] A. Johnson-Buck, J. Nangreave, S. Jiang, H. Yan, N.G. Walter, Nano Lett. 13 (2013) 2754–2759.
[16] R. Jungmann, C. Steinhauer, M. Scheible, A. Kuzyk, P. Tinnefeld, F.C. Simmel, Nano Lett. 10 (2010) 4756–4761.
[17] A. Johnson-Buck, J. Nangreave, D.-N. Kim, M. Bathe, H. Yan, N.G. Walter, Nano Lett. 13 (2013) 728–733.
[18] N.G. Walter, C.-Y. Huang, A.J. Manzo, M.A. Sobhy, Nat. Methods 5 (2008) 475–489.
[19] J. Li, W. Zheng, A.H. Kwon, Y. Lu, Nucleic Acids Res. 28 (2000) 481–488.
[20] N. Michelotti, C. de Silva, A.E. Johnson-Buck, A.J. Manzo, N.G. Walter, Methods Enzymol. 475 (2010) 121–148.
[21] C. Steinhauer, R. Jungmann, T.L. Sobey, F.C. Simmel, P. Tinnefeld, Angew. Chem. Int. Ed. 48 (2009) 8870–8873.
[22] M. Guizar-Sicairos, S.T. Thurman, J.R. Fienup, Opt. Lett. 33 (2008) 156–158.
[23] R.E. Thompson, D.R. Larson, W.W. Webb, Biophys. J. 82 (2002) 2775–2783.
[24] L.S. Churchman, Z. Ökten, R.S. Rock, J.F. Dawson, J.A. Spudich, Proc. Natl. Acad. Sci. USA 102 (2005) 1419–1423.
[25] Y. Tian, Y. He, Y. Chen, P. Yin, C. Mao, Angew. Chem. Int. Ed. 44 (2005) 4355–4358.
[26] Y. He, D.R. Liu, Nat. Nanotechnol. 5 (2010) 778–782.
[27] D.-N. Kim, F. Kilchherr, H. Dietz, M. Bathe, Nucleic Acids Res. 40 (2012) 2862–2868.
[28] C. Lin, R. Jungmann, A.M. Leifer, C. Li, D. Levner, G.M. Church, et al., Nat. Chem. 4 (2012) 832–839.